# Constraints on Warm Dark Matter Mass from Lyman-$\alpha$ forest

Jong Min Yoon

SLAC / Stanford University

**Abstract**

Although the ΛCDM paradigm has shown a remarkable success, there are two conspicuous conflicts between simulations and actual observations: 1) cusp in the halo profile, 2) the large number of subhaloes. Warm Dark Matter is a viable solution for the two problems, keeping the same large scale structures but suppressing the small scale structures. The Lyman-$\alpha$ forest is a powerful probe of the linear power spectrum on these small scales. We use Eulerian N-body hydrodynamics simulations to follow the evolution of WDM models. We compare the artificial Lyman-alpha spectra depending on the mass of the dark matter particles and check whether there really appears the difference in small scale features of the spectra. We argue that careful comparison of the actual observation and simulation can give us a lower bound on the WDM mass.

## 1 Introduction

It is now well established that the Universe is close to flat and matter accounts for about 30 percent of the total energy density. However, ordinary matter is only one fifth of the entire matter content and the majority of matter is expected to be composed of Dark Matter. Among the different DM models, Cold Dark Matter (CDM) models have shown remarkable agreements with what is actually observed and therefore CDM paradigm is now widely accepted as a part of the Standard Model of Cosmology.

However, high resolution N-body simulations of the CDM models have shown two major conflicts with observations. First, although the profile of DM halos is inferred to be shallow from the rotation curves of dwarfs and low surface brightness galaxies,

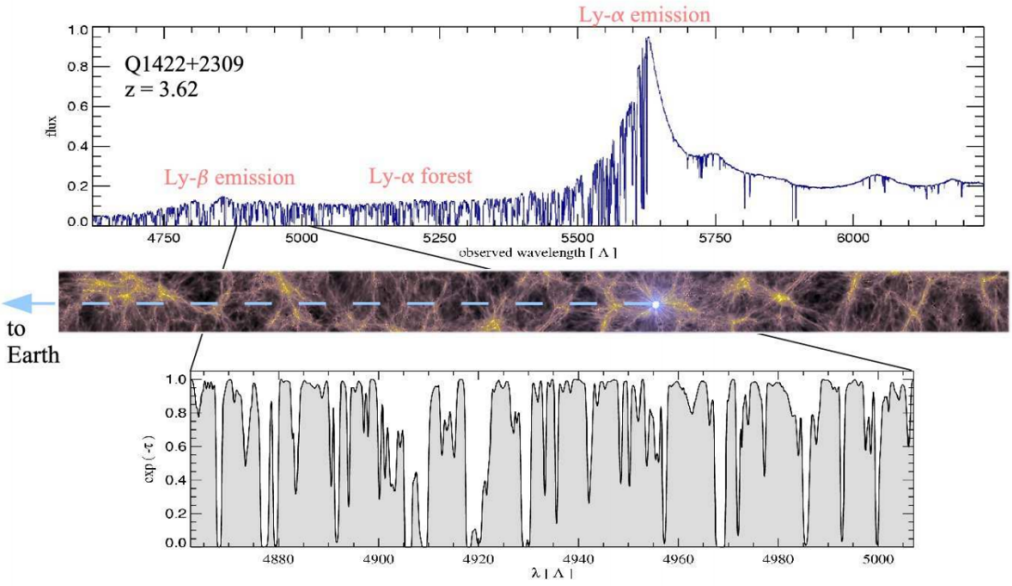


Figure 1: The top panel shows the optical spectrum of the QSO 1422+2309, with a zoom of a small portion of it shown at the bottom. Source: Springel, Volker et al. Nature 440 (2006) 1137 astro-ph/0604561.

the mass density profile of simulated halos are cuspy [1]. Second, in simulation we see a large number of subhalos, which is well above of the observed number of satellite galaxies in the Local Group [2]. These are all small scale structures, and a variety of models has been introduced to reduce the clustering of mass on small scales and solve the conflicts. In particular, Warm Dark Matter model can alleviate the apparent tensions of CDM models with observations. Here, the linear power spectrum is exponentially suppressed on scales smaller than the free-streaming length of the WDM. Due to the much smaller mass of WDM compared to CDM, WDM particles have a considerable thermal velocity and the resulting 'free-streaming' eliminates the density fluctuations of the scales below the free-streaming length, which is roughly given by

$$k_{FS} = \frac{2\pi}{\lambda_{FS}} = 5\mathrm{Mpc}^{-1} \left(\frac{m_x}{1\mathrm{keV}}\right) \left(\frac{T_\nu}{T_x}\right) \frac{2}{3} \tag{1}$$

see e.g. [3].

Then, how can we measure the power spectrum of the small scales? On large scales, the *Planck* mission has provided enormous amounts of data, but on scales below a few comoving Mpc, we have only limited methods of measurement. One possible probe of the matter power spectrum on small scales is Lyman-$\alpha$ forest (See

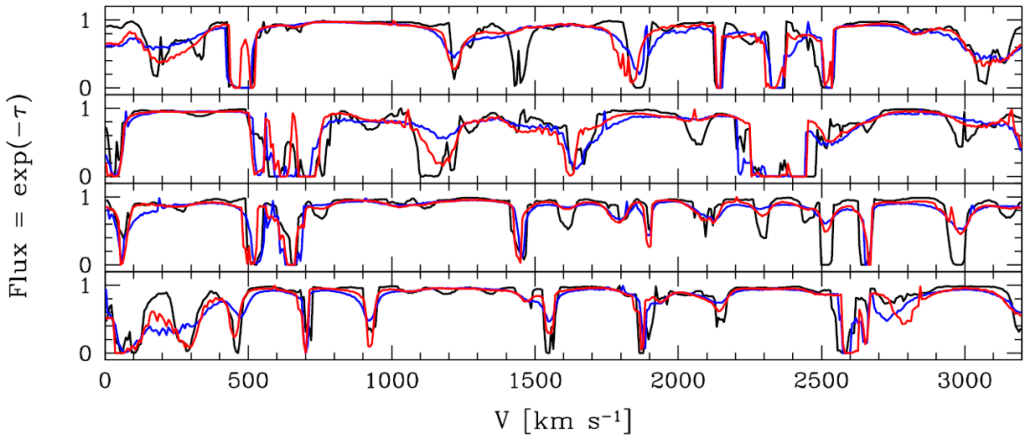


Figure 2: The simulated Lyman-$\alpha$ spectrum in Ref. [4]. Black line shows results for CDM, blue line for WDM with mass 750eV, and red line for WDM with mass 500eV. We can see that blue and red lines have fewer 'small wriggles' compared to the black line, which corresponds to suppressed small scale structures in WDM models.

Fig. 1). Seen in the spectra of high redshift QSOs and galaxies, the Lyman-$\alpha$ forest is produced by intergalactic neutral hydrogen. The original Lyman-$\alpha$ line, which is of wavelength 1216Å, is redshifted depending on the distance of the light source. Furthermore, on its way to us the light of the source passes through intervening neutral hydrogen in the IGM and as the neutral hydrogen absorbs the light, we see a forest of hundreds of sharp absorption lines, depending on the structure of IGM and its distance from us. The typical range of the redshift of QSOs of observed Lyman-$\alpha$ forest are 2-4, and therefore, studying the characteristics of the Lyman-$\alpha$ forest provides us a powerful tool to investigate the scales of interest regarding the viability of WDM model.

The idea of using Lyman-$\alpha$ forest to constrain WDM mass is first introduced in Ref. [4]. Using the N-body simulation of the dark matter and assuming that the baryon contents trace the DM distribution, they compared the simulated Lyman-$\alpha$ spectrum (See Fig. 2) with Keck HIRES observations [5] and conclude that the lower bound of the WDM mass consistent with the observed flux power spectrum is 750eV. Since then, there have been a few other studies improving this method [6, 7] and the current best lower limit of the WDM mass is 3.3keV.

In this study, we generate artificial Lyman-$\alpha$ forest using full hydrodynamics simulation and compare the Lyman-$\alpha$ spectrum of different DM masses, 100GeV, 100keV,

and 1keV. As the main purpose of this final project is to learn computational methods in dark matter study, we provide the procedures of simulation in detail. In Section 2, we explain how we obtain the initial power spectrum at $z = 20$ using CAMB. A transfer function will be introduced to generate different power spectra for WDM models. In Section 3, we provide the details of our simulation - Euler equations and Particle Mesh method. Using the initial power spectrum at $z = 20$, we evolve the system to $z = 3$. The main effort in this section was on expanding the 1D Eulerian simulation discussed in class to full 3D case, and how to incorporate this with PM dark matter evolution. Also, modifications of the code for cosmological simulation(i.e. taking the expansion of universe into account) will be explained too. In Section 4, with the baryon distribution at $z = 3$, we obtain the mock Lyman-$\alpha$ spectrum. In Section 5, we discuss the result and limit of our simulation and possible improvements.

# 2 Initial Matter Power Spectrum

We use the cosmological parameters consistent with Planck 2015 analysis: $H_0 = 67km/s/\text{Mpc}$, $\Omega_b h^2 = 0.022$, $\Omega_m h^2 = 0.12$. We will start with the system at $z = 20$ and evolve to $z = 3$, and we generate the initial matter power spectrum of CDM model at $z = 20$ using CAMB [8]. As mentioned in the Introduction, WDM has smaller mass than CDM and therefore has bigger thermal velocity and longer free-streaming length. The effect of the free streaming on the matter distribution in WDM models can be described by a relative 'transfer function' $T(k)$,

$$P(k)_{WDM} = P(k)_{\Lambda CDM} T(k)^2 \tag{2}$$

In the case when the WDM particles constitute all the dark matter content of the universe. the transfer function can be approximated by the fitting function [6]

$$T(k) = (1 + (\alpha k)^{2\nu})^{-5/\nu} \tag{3}$$

where $\alpha$, the scale of the suppression, is a function of WDM parameters, most importantly its mass. Note for small $k$, the transfer function is very close to 1. The best fit value of $\nu$ for $k < 5h\text{Mpc}^{-1}$ found in the Ref. [6] is $\nu = 1.12$ and for $\alpha$

$$\alpha = 0.049 \left(\frac{m_x}{1\text{keV}}\right)^{-1.11} \left(\frac{\Omega_x}{0.25}\right)^{0.11} \left(\frac{h}{0.7}\right)^{1.22} h^{-1}\text{Mpc} \tag{4}$$

We can see that as $m_x$ increases, $\alpha$ decreases and therefore $T(k)$ is more and more close to 1. The matter power spectrum generated by CAMB for CDM(100GeV) and

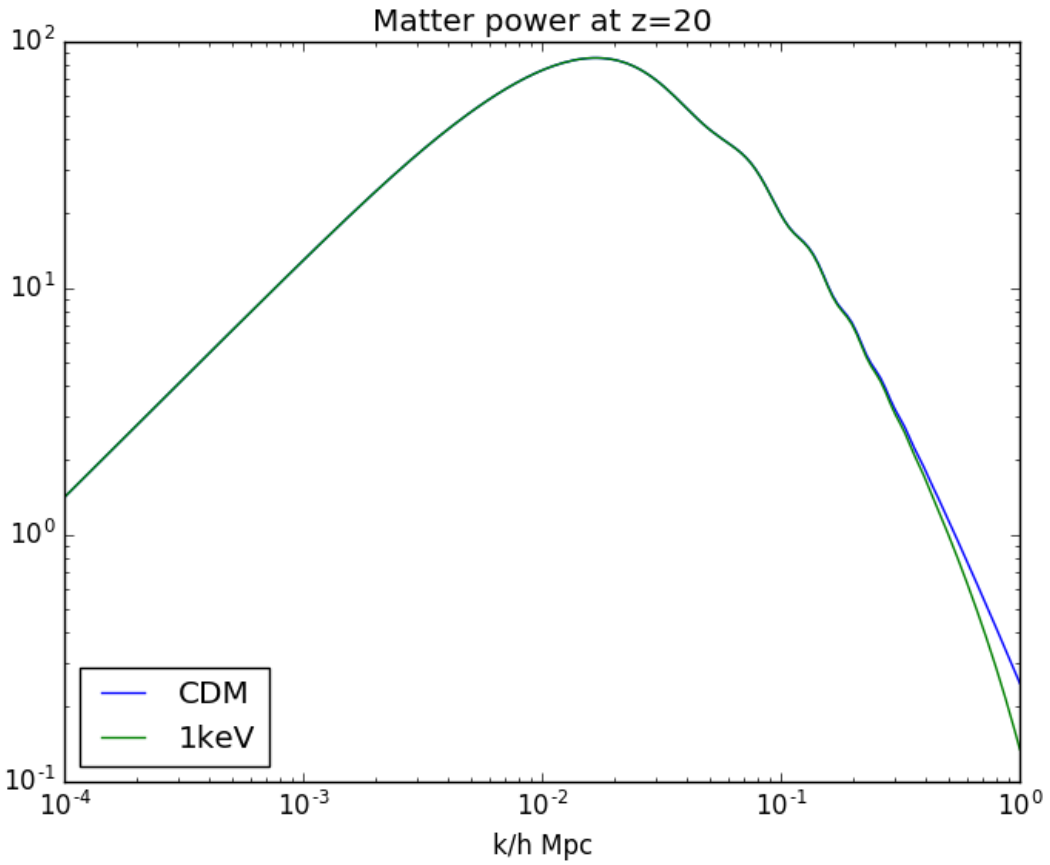


Figure 3: The matter power spectrum of CDM(100GeV) at $z = 20$ obtained from CAMB, and the calculated power spectrum for WDM of mass 1keV from the equations (2)-(4). Note the suppression of WDM power spectrum in small scales.

1keV WDM case is shown in Fig. 3. As we can see, the two matter power spectra are practically identical in larges scales but show difference in small scales.

At the beginning of the simulation (of which details will be discussed in the section below), we deposit dark matter particles using the matter power spectrum of each DM mass. For the baryon part, we set the initial baryon fluid mass densities to be uniform across the grid. Although such a baryon distribution is not realistic, we expect that the baryons will fall into the potential well of the dark matter soon after we begin our hydrodynamics simulation and therefore except a few early steps after $z = 20$, the baryon fluid will have realistic distribution influenced by the DM distribution.

# 3 Hydrodynamic Simulation

## 3.1 3D Eulerian hydrodynamics code

We employ a particle-mesh (PM) N-body simulation and Eulerian hydrodynamics code to evolve the system from $z = 20$ to $z = 3$. The main effort in this part, beyond what is covered in the class, is implementing full 3D Eulerian hydrodynamics code. In this section, we describe how to write the code. Further details and description of other methods can be found in the Enzo documentation [6].

First, the equations of three-dimensional hydrodynamics can be written as,

$$\frac{\partial \mathbf{U}}{\partial t} + \frac{\partial \mathbf{F}}{\partial x} + \frac{\partial \mathbf{G}}{\partial y} + \frac{\partial \mathbf{H}}{\partial z} = \mathbf{R} \tag{5}$$

where, the conserved variable $\mathbf{U}$, the flux in $x$-direction $\mathbf{F}$, the flux in $y$-direction $\mathbf{G}$, the flux in $z$-direction $\mathbf{H}$, and the term $\mathbf{R}$ related to external potential acceleration are

$$\mathbf{U} = \begin{pmatrix} \rho \\ E \\ \rho v_x \\ \rho v_y \\ \rho v_z \end{pmatrix}, \quad \mathbf{R} = \begin{pmatrix} 0 \\ \rho \vec{v} \cdot \vec{g} \\ \rho g_x \\ \rho g_y \\ \rho g_z \end{pmatrix} \tag{6}$$

$$\mathbf{F} = \begin{pmatrix} \rho v_x \\ (E+P)v_x \\ \rho v_x^2 + P \\ \rho v_x v_y \\ \rho v_x v_z \end{pmatrix}, \quad \mathbf{G} = \begin{pmatrix} \rho v_y \\ (E+P)v_y \\ \rho v_x v_y \\ \rho v_y^2 + P \\ \rho v_y v_z \end{pmatrix}, \quad \mathbf{H} = \begin{pmatrix} \rho v_z \\ (E+P)v_z \\ \rho v_x v_z \\ \rho v_y v_z \\ \rho v_z^2 + P \end{pmatrix}, \tag{7}$$

Note that the total energy density is given by $E = \rho e + \frac{1}{2}(v_x^2 + v_y^2 + v_z^2)$.

Using the method of lines, the time dependent evolution of $\mathbf{U}$ can be expressed in the semi-discrete form

$$L(\mathbf{U}^n_{i,j,k}) = -\frac{\mathbf{F}^n_{i+1/2,j,k} - \mathbf{F}^n_{i-1/2,j,k}}{\Delta x} - \frac{\mathbf{G}^n_{i,j+1/2,k} - \mathbf{G}^n_{i,j-1/2,k}}{\Delta y} - \frac{\mathbf{H}^n_{i,j,k+1/2} - \mathbf{H}^n_{i,j,k-1/2}}{\Delta x} + \frac{\mathbf{R}^n_{i,j,k} + \mathbf{R}^{n+1}_{i,j,k}}{2} \tag{8}$$

where $\mathbf{F}^n_{i\pm1/2,j,k}$, $\mathbf{G}^n_{i,j\pm1/2,k}$, and $\mathbf{H}^n_{i,j,k\pm1/2}$ are the fluxes at the time step $n$ and at the cell interface for $x$-, $y$-, and $z$-direction, respectively. As covered in class, these left and right states can be obtained using approximate Riemann solvers, e.g. HLL Riemann solver.

Now, with the obtained $L(\mathbf{U}^n_{i,j,k})$, the time integration can be done using the first-order forward Euler method,

$$\mathbf{U}^{n+1}_{i,j,k} = \mathbf{U}^n_{i,j,k} + \Delta t L(\mathbf{U}^n_{i,j,k}) \tag{9}$$

In the actual cosmological simulation, we need to take into account the expanding universe. In the comoving coordinates, the modified version of equation (5) in the expanding universe is

$$\frac{\partial \mathbf{U}}{\partial t} + \frac{1}{a}\frac{\partial \mathbf{F}}{\partial x} + \frac{1}{a}\frac{\partial \mathbf{G}}{\partial y} + \frac{1}{a}\frac{\partial \mathbf{H}}{\partial z} = \frac{1}{a}(\mathbf{R} + \mathbf{Q}) \tag{10}$$

where $\mathbf{Q} = (0, -2\dot{a}E, \dot{a}\rho v_x, \dot{a}\rho v_y, \dot{a}\rho v_z)$ is an extra term due to the time-dependent scale factor. Here we can see that it is easy to modify the above equations (8) and (9); that is, simply add $\mathbf{Q}$ to $\mathbf{R}$ and use $dt \to dt/a$.

## 3.2 Evolution of the system from $z = 20$ to $z = 3$

Now fully equipped with PM code for dark matter evolution and Eulerian hydrodynamics code for baryon fluid evolution, we can evolve the system from $z = 20$ to $z = 3$. Incorporating the PM code, each iteration of the evolution looks like this:

1) Make sure DM particle distribution is within the box range. If not, change the particle locations using the periodicity of the simulation volume,

2) Deposit DM particles in the force mesh. Here we use Cloud-In-Cell interpolation scheme.

3) Add the baryon densities, and make sure the mean of the density distribution is zero, as we are working in periodic volume.

4) Compute potential in the force mesh from the densities.

5) Compute acceleration field in the force mesh, from the potential. Note this field will be used in $\mathbf{R}$ of the Eulerian evolution.

6) From the acceleration field, calculate the acceleration for each DM particles.

7) Evolve the position and velocity of DM particles, using the Leapfrog scheme. Note in cosmological simulation, we use $dt/a$ instead of $dt$. We choose $a$ for each drift and kick by its value at the middle of the each drift/kick time step.

8) Now for baryon fluid, compute $L(\mathbf{U}^n_{i,j,k})$ using HLL Riemann Solver and the acceleration field computed in the step 5.

9) Update $\mathbf{U}$, using $L(\mathbf{U}^n_{i,j,k})$. Again, we use $dt/a$ instead of $dt$.

10) Obtain $\rho$, $v$ and $E$ back from the updated $\mathbf{U}$.

Again, we evolve the system from $z = 20$ to $z = 3$. This corresponds to the initial internal time $t_{start} = 0.809$ and the final internal time $t_{final} = 9.736$. Although we have implemented full 3D code, for the purpose of the subsequent simulation we use 2D grid: our periodic simulation volume has $N_p = 80^2$ particles and $N_m = 100^2$ force mesh. For this system, the typical number of iterations from $z = 20$ to $z = 3$ is 1270. Finally, although we have made efforts on correctly incorporating scale factor and implementing physical unit system in the simulation, there seems to be remaining errors in that regard. Therefore, although it is true that the results of simulation and analysis below is qualitatively correct, the exact quantitative values of the remaining parts of this report should be taken with caution. The typical evolution process is shown in Fig. 4.

# 4 Getting Lyman-$\alpha$ Spectra

From the baryon distribution at $z = 3$ obtained in Section 3, we extract artificial Lyman-$\alpha$ spectra along a random line of sight through the simulation volume. First, we compute the baryon overdensity along a randomly chosen line of sight. To overcome the limitation of small simulation volume, we can utilize the periodicity assumption and lengthen the effective simulation volume by scanning the grid several times. In order to avoid strictly periodic signal due to this practice, we choose the direction of our line of sight to be of the angle $\tan^{-1}(\pi/2)$ in $x - y$ plane. However, certain amount of 'approximate' periodicity is inevitable in this scheme, as one can easily anticipate.

In order to get the artificial Lyman-$\alpha$ spectra , we need the optical depth along the line of sight from the overdensity. Here we employ the Fluctuating Gunn-Peterson Approximation [10], which makes use of the power-law temperature density relation and describes the relation between Lyman-$\alpha$ opacity and baryon overdensity as fol-

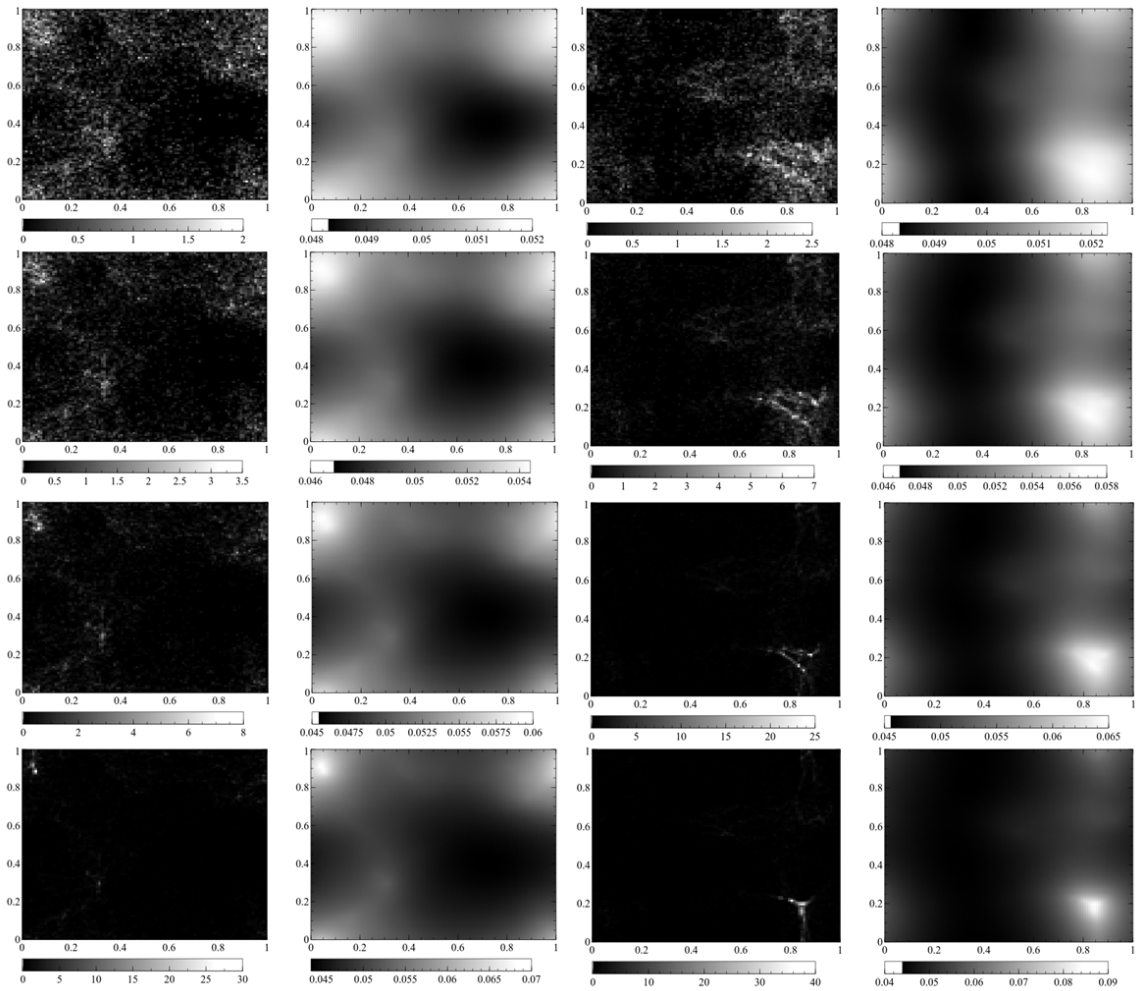

Figure 4: The sample evolution of the 2D system described in Section 3.2. The left two columns are of CDM case (100GeV), and the right two columns are of WDM with mass 100keV. For each mass, images in the left column show the evolution of DM particles, and those in the right column show the evolution of baryons. From the top to bottom, the corresponding redshifts are $z = 11.42$, 6.83, 4.97, 3.92. Note that although baryons started with uniform distribution, they quickly fall into the potential well of DM.

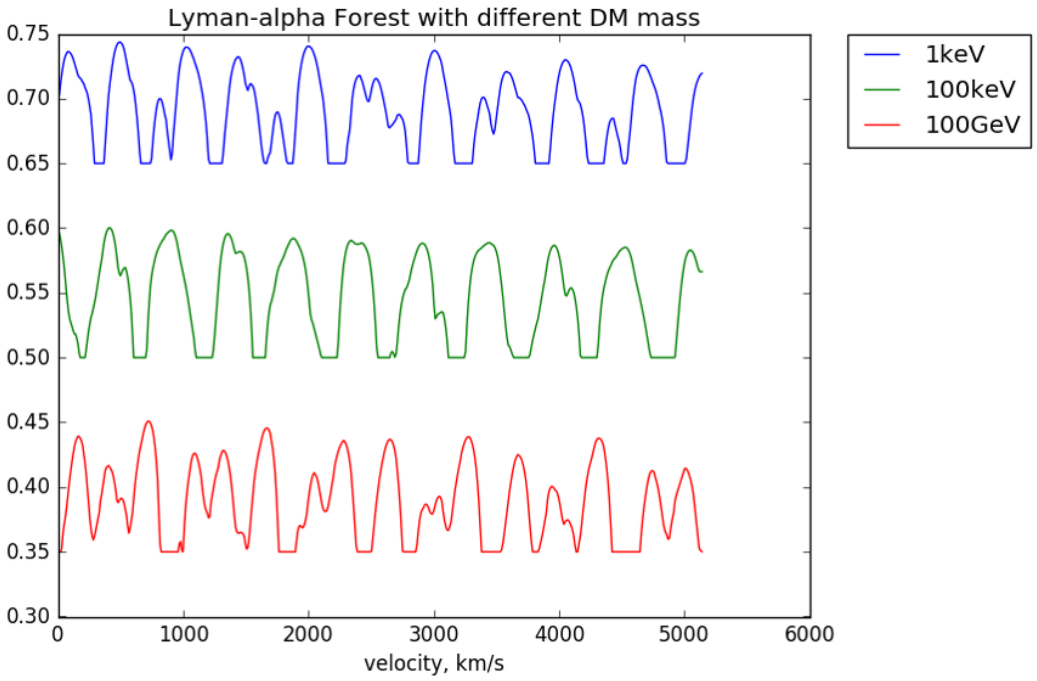


Figure 5: The artificial Lyman-$\alpha$ Spectra of two WDM models and CDM. All the three spectra are in the same scale, but transposed for the better visual comparison. Note that as mentioned in Section 4, we see the approximate periodicity in the spectra due to our scheme of line of sight.

lows:

$$\tau(z) = A(z)(1+\delta_b(z))^{1.7}$$
$$A(z) = 0.433\left(\frac{1+z}{3.5}\right)^6\left(\frac{\Omega_b h^2}{0.02}\right)^2\left(\frac{T_0}{6000K}\right)^{-0.7}\times$$
$$\left(\frac{h}{0.65}\right)^{-1}\left(\frac{H(z)/H_0}{3.68}\right)^{-1}\left(\frac{\Gamma_{HI}}{1.5\times10^{-12}\mathrm{s}^{-1}}\right)$$

$\Gamma_{HI}$ is the HI photoionization rate.

Finally, we obtain the artificial Lyman-$\alpha$ Spectra of two WDM models with DM mass 1keV and 100keV, and CDM with mass 100GeV (Fig. 5).

# 5 Discussion and Conclusion

At the beginning of this study, we expected that as the small scale structures are suppressed in WDM models, the smaller the dark matter mass is, the smoother the

Lyman-$\alpha$ spectrum is. However, what we see in the simulated Lyman-$\alpha$ spectrum in Fig. 5 seems not fully consistent with our expectation. Although it is rather fair to say that 100keV spectrum is smoother than 100GeV spectrum, we see in 1keV spectrum more wriggles than 100keV spectrum, and comparable to 100GeV spectrum. There can be many different reasons of inaccuracy of our simulation. First, if we have generated the artificial Lyman-$\alpha$ spectrum with much more statistics by performing more number of simulations and extracting more number of line of sight, we would have seen more consistent results with the previous studies in Refs. [4, 5, 6]. Second, if we use bigger box size, we can reduce the approximate periodicity in the spectra and get more realistic spectra. Indeed, what we want to see in this study is the changes in small scale structures in Lyman-$\alpha$ spectra according to WDM mass, and to see the small scale structures in the spectra it is important to have a very fine resolution. With the current grid size, we have not achieved such resolution yet. Third, as mentioned in section 3, our physical unit system is not fully correct yet and also there could be still remaining errors of missing scale factors in simulation. Fourth, rather than using the Fluctuating Gunn-Peterson Approximation, if we use more thorough analysis of extracting optical depth from the baryon density distribution, the agreement of our artificial spectra to the physical ones will be better. For example, we can express the absorption cross section in terms of a Voigt function and incorporate the peculiar velocity information upto the first order in $v/c$ when calculating the optical depth at each wavelength. With all those improvements, we expect that we can really see that the spectra from WDM models is smoother than that of CDM model. When equipped with simulation method of such precision, we can really compare the artificial spectra with what is actually observed, e.g. Keck HIRES data. Careful comparison of the simulation and observation then lead to the lower bound on WDM mass.

## Acknowledgments

The author is grateful to Prof. Tom Abel for discussions and email correspondences on various aspects of implementing hydrodynamics code and Lyman-$\alpha$ spectra. This work is done as a final project of Physics 368 Computational Cosmology, Winter 2016 at Stanford University.

# References

[1] Moore, B. Nature 370 (1994) 629; de Blok, W.J.G. et al. Mon.Not.Roy.Astron.Soc. 290 (1997) 533-552 astro-ph/9704274; Hernandez, X. et al. Mon.Not.Roy.Astron.Soc. 294 (1998) 595 astro-ph/970916; P. Bode, J. P. Ostriker and N. Turok, Astrophys. J. 556, 93 (2001)

[2] Klypin, Anatoly A. et al. Astrophys.J. 522 (1999) 82-92 astro-ph/9901240, Moore, B. et al. Astrophys.J. 524 (1999) L19-L22 astro-ph/9907411

[3] J. R. Bond, G. Efstathiou and J. Silk, Phys. Rev. Lett. 45, 1980 (1980).

[4] Narayanan, Vijay K.; Spergel, David N.; Dave, Romeel; Ma, Chung-Pei, Astrophys. J. 543, 103 (2000).

[5] Vogt, S. S., Allen, S. L., Bigelow, B. C., et al. 1994, Proc. SPIE, 2198, 362.

[6] Viel, Matteo et al., Phys. Rev. D 71, 063534 (2005).

[7] Viel, Matteo et al. Phys.Rev. D88 (2013) 043502.

[8] Lewis, Antony; Challinor, Anthony; Lasenby, Anthony, ApJ, 538, 473 (2000).

[9] ENZO Collaboration (Bryan, Greg L. et al.) Astrophys.J.Suppl. 211 (2014) 19.

[10] J. E. Gunn and B. A. Peterson, Astrophys. J. 142, 1633 (1965).